AIAA JOURNAL
Vol. 35, No. 11, November 1997

Quantitative Prediction of Thermomechanical Coupling Effect in Thermo–Elasto–Viscoplastic Composite Materials

Eui-Sup Shin* and Seung-Jo Kim†
Seoul National University, Kwanak-Ku, Seoul 151-742, Republic of Korea

Thermo–elasto–viscoplastic analyses are performed to view the thermomechanical coupling effect in composite materials subjected to quasistatic and dynamic loads. An unmixing-mixing scheme is utilized to describe the thermo–elasto–viscoplastic characteristics of orthotropic composites. The equation of motion and the energy conservation equation based on fully coupled thermomechanics are formulated with constitutive arrangement by the unmixing–mixing concept. By considering some auxiliary conditions, the initial-boundary value problem is completely set up. In computational aspects, the governing equations are reformulated with the finite element method, and then the time marching techniques fit for the full discretization are applied. To solve the ultimate nonlinear equations, the successive iteration algorithm is constructed with a subincrementing technique. Finally, numerical examples are presented to show the fundamental trends of the thermo–elasto–viscoplastic behavior of composite laminates. The progress of viscoplastic deformation and the temperature change owing to the coupling effect are carefully examined when the composite laminates are subjected to repeated cyclic loading.

Nomenclature

$\boldsymbol{A}$	= elastic compliance tensor
$\boldsymbol{B}, \boldsymbol{C}, \boldsymbol{D}$	= fourth-order tensors in the unmixing–mixing equations
$[B]$	= interpolation matrix for strain or temperature gradient
$[H]$	= interpolation matrix for displacement or temperature
$\boldsymbol{S}$	= deviatoric stress tensor
$\boldsymbol{t}$	= traction vector
$\{U\}$	= nodal point displacement
Z	= internal state variable
$\boldsymbol{\alpha}$	= thermal expansion tensor
$\boldsymbol{\beta}$	= second-order tensor in the unmixing–mixing equations
$\boldsymbol{\kappa}$	= thermal conductivity tensor
$\{\Theta\}$	= nodal point temperature
θ, θ_0	= current temperature and base temperature
θ_+	= temperature change $(\theta - \theta_0)$
ξ	= dissipation factor of viscoplastic work
$(\dot{}), (\ddot{})$	= time derivatives

Subscripts

$[f], [m], [m_i]$	= fiber, matrix, and ith matrix partition
U, Θ	= variable related to displacement or temperature

Superscripts

$(i), (i+1)$	= iteration indices (left-hand side)
p	= viscoplastic component
$t, t + \Delta t$	= current and following time (left-hand side)

Introduction

COMPOSITE materials have been used successfully in severe mechanical and/or thermal environment for various aerospace applications.[1] Recently, for example, the interest in hypersonic vehicles has brought attention to advanced materials because structural components are operated under extremely severe aerothermal conditions.[2] It is known that thermoplastic and metal–matrix composites may experience an appreciable amount of viscoplastic deformation, especially at high temperatures.

In general, the inherent anisotropy of composites increases the difficulty in describing the viscoplastic deformation. To date, many kinds of constitutive theories have been suggested to simulate the viscoplastic response of the anisotropic materials. Most of the theories were modified and extended from the classical plasticity models or the unified viscoplastic models for isotropic materials by introducing macroscopic composite mechanics.[3–7] On the other hand, there have been several efforts made based on micromechanics, which predicts the overall behavior of composite from the individual properties of constituent materials.[8–12] Recently, Kim and Cho[11] and Kim and Shin[12] proposed an unmixing–mixing concept and considered a general procedure to systematically analyze the viscoplastic behavior of composites. The scheme was extended by the multipartite matrix method, which enables one to handle some microstructural effect due to heterogeneity.[12]

To accurately solve the complex thermomechanical problems, in principle, all of the governing equations in continuum mechanics must be solved simultaneously because the mechanical fields and the thermodynamic fields are coupled interactively. Accordingly, as summarized in Table 1, there are three types of mathematical formulation that depend on the treatment of thermomechanical field variables.

It is recognized that the coupling between mechanics and thermodynamics has a weak effect on the behavior of elastic materials, and one-way coupled formulation is sufficient for the thermoelastic problems. But the coupling effect is not always negligible for viscoplastic materials, especially when the materials are used repeatedly under cyclic loads. With the development of viscoplastic deformation, generally, a certain portion of mechanical energy is converted to heat, thus resulting in an irreversible rise in temperature. As a result, mechanical variables such as displacement and stress are also changed interactively. Until now, numerical analyses with the fully coupled formulation have been performed by several researchers.[13–19] However, to the authors' knowledge, the numerical results were limited to isotropic materials. Therefore, the quantitative prediction of thermomechanical coupling effect in viscoplastic composites is necessary to accurately analyze the behavior of composite structures operated under intense surrounding conditions.

In this paper, the finite element formulation that enables the fully coupled thermomechanical analysis is presented. The unmixing–mixing scheme is adopted to represent the constitutive relationship of orthotropic composites. The equation of motion and the energy

Received Oct. 7, 1996; revision received April 4, 1997; accepted for publication July 3, 1997.

*Postdoctoral Researcher, Department of Aerospace Engineering. Member AIAA.
†Professor, Department of Aerospace Engineering. Member AIAA.

Table 1 Three types of thermomechanical formulation in continuum mechanics

Mechanical fields	Coupling type (interrelation)	Thermodynamic fields
Stress, strain, viscoplastic strain, displacement, etc.	1) Uncoupled (×) 2) One-way coupled (⇤⇥) 3) Fully coupled (⇤⇥)	Temperature, heat flux, energy, entropy, etc.

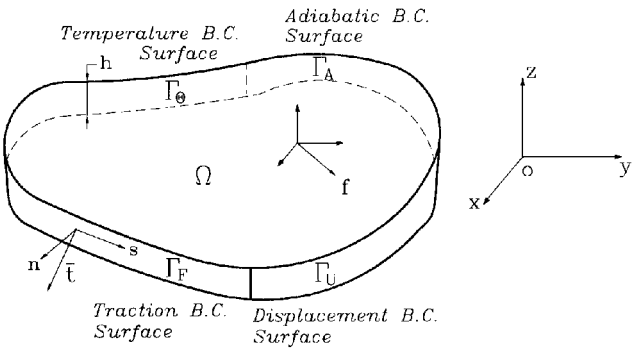

Fig. 1 Geometric configuration of a composite laminate and its boundaries.

conservation equation are considered, together with the constitutive arrangement by the unmixing–mixing concept. By considering auxiliary conditions, the initial-boundary value problem is completely set up. In computational aspects, the governing equations are reformulated with the finite element method. The derived nonlinear equations are fully discretized in incremental forms. As a numerical study, a series of analyses are performed with the focus on the coupling effect in the metal matrix composite. The development of viscoplastic deformation, the stress–strain relation, and the temperature change are carefully examined when the composite laminates are cyclically subjected to static and dynamic loads.

Governing Equations with Auxiliary Conditions

The governing equations are briefly summarized in tensor notation. As shown in Fig. 1, the thin laminates, which infinitesimally deform in a plane, are treated.

1) Equation of motion:

$$\nabla \cdot \boldsymbol{\sigma} + \bar{\boldsymbol{f}} = \rho \ddot{\boldsymbol{u}} \tag{1}$$

2) Energy conservation equation:

$$\rho c_v \dot{\theta}_+ = -\theta \boldsymbol{\alpha} : \boldsymbol{A}^{-1} : (\dot{\boldsymbol{\varepsilon}} - \dot{\boldsymbol{\varepsilon}}^p) + \xi \boldsymbol{\sigma} : \dot{\boldsymbol{\varepsilon}}^p + \nabla \cdot (\boldsymbol{x} \cdot \nabla \theta_+) \tag{2}$$

By applying the principles of thermodynamics (energy conservation and entropy production),[20] Eqs. (2) are derived for a class of viscoplastic composites. The terms on the right-hand side are the contribution to thermal energy by the reversible thermoelastic deformation, the dissipative viscoplastic deformation, and the irreversible heat conduction, respectively.

3) Strain-displacement relation:

$$\boldsymbol{\varepsilon} = \tfrac{1}{2}[\nabla \cdot \boldsymbol{u} + (\nabla \cdot \boldsymbol{u})^T] \tag{3}$$

4) Constitutive equation; unmixing–mixing scheme:

$$\dot{\boldsymbol{\varepsilon}} = \boldsymbol{A}\dot{\boldsymbol{\sigma}} + \boldsymbol{\alpha}\dot{\theta}_+ + \dot{\boldsymbol{\varepsilon}}^p \tag{4}$$

$$\dot{\boldsymbol{\varepsilon}}^p = \sum_{k=1}^{N} \boldsymbol{B}_{[m_k]} \dot{\boldsymbol{\varepsilon}}^p_{[m_k]} \tag{5}$$

$$\dot{\boldsymbol{\sigma}}_{[f]} = \boldsymbol{C}_{[f]}\dot{\boldsymbol{\sigma}} + \boldsymbol{\beta}_{[f]}\dot{\theta}_+ + \sum_{k=1}^{N} \boldsymbol{D}_{[fk]} \dot{\boldsymbol{\varepsilon}}^p_{[m_k]} \tag{6}$$

$$\dot{\boldsymbol{\sigma}}_{[m_i]} = \boldsymbol{C}_{[m_i]}\dot{\boldsymbol{\sigma}} + \boldsymbol{\beta}_{[m]}\dot{\theta}_+ + \sum_{k=1}^{N} \boldsymbol{D}_{[m_{ik}]} \dot{\boldsymbol{\varepsilon}}^p_{[m_k]} \tag{7}$$

which are the extended unmixing–mixing equations[11,12]; that is, the strain rate equation, the overall viscoplastic flow law, the fiber stress equation, and the matrix stress equation.

Tensor $\boldsymbol{B}$ in Eq. (5) relates the viscoplastic deformation of the ith matrix to the overall viscoplastic response of the composite by linear transformation. In other words, Eq. (6) means that the overall plastic strain rate is contributed by the viscoplastic strain rate of each matrix partition in the micromechanical model,[12] which consists of one fiber and neighboring matrix. Tensor $\boldsymbol{B}$ is expressed in matrix form in the Appendix. Three terms on the right-hand side of Eq. (6) or (7) stand for the corresponding microstress, which is the stress of the fiber in the micromechanical model, contributed from the overall loading, the thermal expansion, and the matrix viscoplasticity, respectively. The deformed state in the matrix is represented with a set of variables for the N parts of the matrix. The tensors can be represented by matrix notations in the principal material coordinates (see the Appendix).

5) Constitutive equation; Bodner–Partom theory:

$$\dot{\varepsilon}^p_{[m_i]} = \frac{D_0}{\sqrt{J_{[m_i]2}}} \exp\left[-\frac{1}{2}\left(\frac{Z^2_{[m_i]}}{3J_{[m_i]2}}\right)^n\right] \boldsymbol{S}_{[m_i]} \tag{8}$$

$$\boldsymbol{S}_{[m_i]} \overset{\text{def}}{=} \boldsymbol{\sigma}_{[m_i]} - \tfrac{1}{3}\mathrm{tr}(\boldsymbol{\sigma}_{[m_i]})\boldsymbol{1} \tag{9}$$

$$\boldsymbol{J}_{[m_i]2} \overset{\text{def}}{=} \tfrac{1}{2}\boldsymbol{S}_{[m_i]} : \boldsymbol{S}_{[m_i]} \tag{10}$$

$$\dot{Z}_{[m_i]} = m_1(Z_1 - Z_{[m_i]})\boldsymbol{\sigma}_{[m_i]} : \dot{\boldsymbol{\varepsilon}}^p_{[m_i]} - A_1 Z_1 \left(\frac{Z_{[m_i]} - Z_2}{Z_1}\right)^{r_1} \tag{11}$$

Any isotropic viscoplastic theory may be applied as the viscoplastic model of the matrix. Here, the constitutive relation proposed by Bodner and Partom is adopted.[21] The summarized expression consists of the flow law and the evolution equation of internal state variable. In Eqs. (8–11), D_0, Z_1, Z_2, m_1, A_1, r_1, and n are the viscoplastic constants of the matrix.

The detailed information on unknowns and equations is listed in Table 2. By prescribing auxiliary conditions together, the initial-boundary value problem is completely defined. The initial conditions are as follows.

1) Initial condition; macromechanical variables:

$$\boldsymbol{\sigma}|_{t=0} = \boldsymbol{0}, \qquad \boldsymbol{\varepsilon}|_{t=0} = \boldsymbol{0}, \qquad \boldsymbol{\varepsilon}^p|_{t=0} = \boldsymbol{0} \tag{12}$$

$$\boldsymbol{u}|_{t=0} = \boldsymbol{0}, \qquad \dot{\boldsymbol{u}}|_{t=0} = \boldsymbol{0}, \qquad \theta_+|_{t=0} = 0 \tag{13}$$

2) Initial condition; micromechanical variables:

$$Z_{[m_i]}\big|_{t=0} = Z_0, \qquad \text{other variables} = 0 \tag{14}$$

The boundary conditions are as follows.

1) Displacement boundary condition on Γ_U:

$$\boldsymbol{u} = \bar{\boldsymbol{u}} \tag{15}$$

2) Traction boundary condition on Γ_F:

$$\boldsymbol{n} \cdot \boldsymbol{\sigma} = \bar{\boldsymbol{t}} \tag{16}$$

3) Temperature boundary condition on Γ_Θ:

$$\theta_+ = \bar{\theta}_+ \tag{17}$$

4) Adiabatic boundary condition on Γ_A:

$$(\boldsymbol{x} \cdot \nabla \theta_+) \cdot \boldsymbol{n} = 0 \tag{18}$$

Finite Element Formulation

Equation of Motion

Variational formulation starting from governing differential equations is performed to solve the fully coupled problems. The principle of virtual work is applied to the equilibrium state with the virtual displacement, which vanishes on Γ_U,

$$\int_\Omega (\nabla \cdot \boldsymbol{\sigma} + \bar{\boldsymbol{f}} - \rho\ddot{\boldsymbol{u}}) \cdot \delta\boldsymbol{u}\, \mathrm{d}\Omega - \int_{\Gamma_F} (\boldsymbol{n} \cdot \boldsymbol{\sigma} - \bar{\boldsymbol{t}}) \cdot \delta\boldsymbol{u}\, \mathrm{d}\Gamma_F = 0 \tag{19}$$

Table 2 List of unknowns and equations in a thermomechanical problem

Number of unknowns		Equation name	Equation no.	No. of equations
Macrolevel variable		Equation of motion	(1)	2
Stress tensor	3	Energy conservation equation	(2)	1
Strain tensor	3	Strain-displacement relation	(3)	3
Displacement vector	2	Constitutive relation (unmixing–mixing scheme)		
Temperature	1	Strain rate equation	(4)	3
Viscoplastic strain tensor	3	Viscoplastic flow law	(5)	3
Microlevel variable		Fiber stress equation	(6)	3
Fiber stress tensor	3	Matrix stress equation	(7)	$N \times 3$
Matrix stress tensor	$N \times 3$	Constitutive equation (Bodner–Partom theory)		
Matrix deviatoric stress tensor	$N \times 4$	Flow law and kinetic equation	(8)	$N \times 3$
Matrix viscoplastic strain tensor	$N \times 3$	Deviatoric stress definition	(9)	$N \times 4$
Matrix deviatoric stress invariant	N	Stress invariant definition	(10)	N
Matrix internal state variable	N	Evolution equation	(11)	N
	$15 + N \times 12$			$15 + N \times 12$

The displacement and the temperature are spatially interpolated with the isoparametric finite elements:

$$\begin{Bmatrix} u(x, y; t) \\ v(x, y; t) \end{Bmatrix} = [H_U(x, y)]\{U(t)\} \tag{20}$$

$$\begin{Bmatrix} \varepsilon_x(x, y; t) \\ \varepsilon_y(x, y; t) \\ \gamma_{xy}(x, y; t) \end{Bmatrix} = [B_U(x, y)]\{U(t)\} \tag{21}$$

$$\theta_+(x, y; t) = [H_\Theta(x, y)]\{\Theta(t)\} \tag{22}$$

$$\begin{Bmatrix} \dfrac{\partial \theta_+}{\partial x}(x, y; t) \\ \dfrac{\partial \theta_+}{\partial y}(x, y; t) \end{Bmatrix} = [B_\Theta(x, y)]\{\Theta(t)\} \tag{23}$$

By using the divergence theorem, the semidiscretized form of the equation of motion can be derived as follows:

$$[M_U]\{\ddot{U}\} + \{F_U\} - \{R_U\} = \{0\} \tag{24}$$

where

$$[M_U] \stackrel{\text{def}}{=} \int_\Omega \rho [H_U]^T [H_U] \, d\Omega \tag{25}$$

$$\{F_U\} \stackrel{\text{def}}{=} \int_\Omega [B_U]^T \{\sigma\} \, d\Omega \tag{26}$$

$$\{R_U\} \stackrel{\text{def}}{=} \int_\Omega [H_U]^T \{\bar{f}\} \, d\Omega + \int_{\Gamma_F} [H_U]^T \{\bar{t}\} \, d\Gamma_F \tag{27}$$

To obtain a fully discretized approximation, the Newmark integration (constant average acceleration) method[22] is applied to Eq. (24):

$$([K_U] + (4/\Delta t^2)[M_U])\{\Delta U\} = \{{}^{t+\Delta t}R_U\} - \{{}^tF_U\} + [A_\Theta]\{\Delta\Theta\} + \{\Delta P_U\} + [M_U]((4/\Delta t)\{{}^t\dot{U}\} + \{{}^t\ddot{U}\}) \tag{28}$$

where

$$[K_U] \stackrel{\text{def}}{=} \int_\Omega [B_U]^T [A]^{-1} [B_U] \, d\Omega \tag{29}$$

$$[A_\Theta] \stackrel{\text{def}}{=} \int_\Omega [B_U]^T [A]^{-1} \{\alpha\} [H_\Theta] \, d\Omega \tag{30}$$

$$\{\Delta P_U\} \stackrel{\text{def}}{=} \int_\Omega [B_U]^T [A]^{-1} \{\Delta \varepsilon^p\} \, d\Omega \tag{31}$$

$$\{\Delta \varepsilon^p\} \stackrel{\text{def}}{=} \int_t^{t+\Delta t} \{\dot{\varepsilon}^P\} \, d\tau \tag{32}$$

Note that the temperature vector is a secondary independent variable in the preceding equations.

Energy Conservation Equation

Next, the Galerkin method[13] is used for the restatement of the energy conservation equation in governing equation (2):

$$\int_\Omega \rho c_v \dot{\theta}_+ \delta\theta \, d\Omega - \int_\Omega \nabla \cdot (\boldsymbol{\kappa} \cdot \nabla \theta_+) \delta\theta \, d\Omega = -\int_\Omega \theta \boldsymbol{\alpha} : \boldsymbol{A}^{-1} : (\dot{\boldsymbol{\varepsilon}} - \dot{\boldsymbol{\varepsilon}}^p) \delta\theta \, d\Omega + \int_\Omega \xi \boldsymbol{\sigma} : \dot{\boldsymbol{\varepsilon}}^p \delta\theta \, d\Omega \tag{33}$$

Through the procedure of finite element discretization, the following is obtained:

$$[M_\Theta]\{\dot{\Theta}\} + [K_\Theta]\{\Theta\} = \{\dot{E}_\Theta\} + \{\dot{P}_\Theta\} \tag{34}$$

where

$$[M_\Theta] \stackrel{\text{def}}{=} \int_\Omega \rho c_v [H_\Theta]^T [H_\Theta] \, d\Omega \tag{35}$$

$$[K_\Theta] \stackrel{\text{def}}{=} \int_\Omega [B_\Theta]^T [x] [B_\Theta] \, d\Omega \tag{36}$$

$$\{\dot{E}_\Theta\} \stackrel{\text{def}}{=} -\int_\Omega \theta [H_\Theta]^T \{\alpha\}^T [A]^{-1} (\{\dot{\varepsilon}\} - \{\dot{\varepsilon}^p\}) \, d\Omega \tag{37}$$

$$\{\dot{P}_\Theta\} \stackrel{\text{def}}{=} \int_\Omega \xi [H_\Theta]^T \{\sigma\}^T \{\varepsilon^p\} \, d\Omega \tag{38}$$

Equation (34) is fully discretized with the Crank–Nicolson technique[23] in a time domain:

$$([M_\Theta] + (\Delta t/2)[K_\Theta])\{\Delta\Theta\} = \{\Delta E_\Theta\} + \{\Delta P_\Theta\} - \Delta t[K_\Theta]\{{}^t\Theta\} \tag{39}$$

where

$$\{\Delta E_\Theta\} \stackrel{\text{def}}{=} -\int_\Omega [H_\Theta]^T \{\alpha\}^T [A]^{-1} \{\Delta\tilde{\varepsilon}\} \, d\Omega \tag{40}$$

$$\{\Delta P_\Theta\} \stackrel{\text{def}}{=} \int_\Omega \xi [H_\Theta]^T \{\Delta w^p\} \, d\Omega \tag{41}$$

$$\{\Delta\tilde{\varepsilon}\} \stackrel{\text{def}}{=} \int_t^{t+\Delta t} \theta(\{\dot{\varepsilon}\} - \{\dot{\varepsilon}^p\}) \, d\tau \tag{42}$$

$$\{\Delta w^p\} \stackrel{\text{def}}{=} \int_t^{t+\Delta t} \{\sigma\}^T \{\dot{\varepsilon}^p\} \, d\tau \tag{43}$$

Computational Algorithm

The resulting equations [Eqs. (28) and (39)] are nonlinear with the fully coupled terms. Therefore, the incremental solutions $\{\Delta U\}$ and $\{\Delta\Theta\}$ are obtained through an iteration process. Fast convergence depends largely on how accurately the nonlinear terms in Eqs. (32), (42), and (43) are calculated. Because of the numerically stiff phenomenon of the viscoplastic rate equations, a subincrementing

technique is adopted at each Gauss integration point.[24] The computational algorithm for the finite element code is as follows.

1) Initialize all of the variables at $t = 0$, and determine Δt.

2) Apply the load increment, and start the iteration stage with $i = 0$.

3) Assemble the matrices in Eq. (28), and solve it to obtain $\{^{(i+1)}\Delta U\}$.

4) Calculate the nonlinear terms in the energy conservation equation by the subincrementing technique:

$$\left\{^{(i)}\Delta\tilde{\varepsilon}\right\} = \int_t^{t+\Delta t} {}^{(i)}\theta\left(\left\{^{(i)}\dot{\varepsilon}\right\} - \left\{^{(i)}\dot{\varepsilon}^p\right\}\right) d\tau \tag{44}$$

$$\left\{^{(i)}\Delta w^p\right\} = \int_t^{t+\Delta t} \left\{^{(i)}\sigma\right\}^T \left\{^{(i)}\dot{\varepsilon}^p\right\} d\tau \tag{45}$$

5) Assemble the matrices in Eq. (39), and solve it to obtain $\{^{(i+1)}\Delta\Theta\}$.

6) Calculate the nonlinear term in the equation of motion by the subincrementing technique:

$$\left\{^{(i)}\Delta\varepsilon^p\right\} = \int_t^{t+\Delta t} \left\{^{(i)}\dot{\varepsilon}^p\right\} d\tau \tag{46}$$

7) Check the convergence criteria with the relative errors:

$$\frac{\left\|\left\{^{(i+1)}\Delta U\right\} - \left\{^{(i)}\Delta U\right\}\right\|}{\left\|\left\{^{(i+1)}\Delta U\right\}\right\|} \le E_{\text{tol}\,U} \tag{47}$$

$$\frac{\left\|\left\{^{(i+1)}\Delta\Theta\right\} - \left\{^{(i)}\Delta\Theta\right\}\right\|}{\left\|\left\{^{(i+1)}\Delta\Theta\right\}\right\|} \le E_{\text{tol}\,\Theta} \tag{48}$$

8) If it converges, update all of the variables to the current values. Return to step 2.

9) If it diverges, increase the iteration index i by one. Return to step 3.

With a slight modification, this algorithm can be applied to other problems. For example, if steps 4 and 5 are skipped, the uncoupled structural analysis can be performed. And by neglecting steps 3 and 6, the equation of unsteady heat conduction for composite laminates can be solved.

Numerical Results and Discussion

Material System

The metal matrix composite, silicon–carbide fiber, titanium alloy matrix (SCS-6/Ti-15-3), is selected as the standard material system in numerical analyses. The material properties are chosen at a high temperature, 815°C. The fiber volume fraction is 0.6, and the unmixing–mixing model has one part of fiber and two parts of matrix ($V_{[m1]} = 0.3$, $V_{[m2]} = 0.1$). The material constants for the respective phases and the overall composite are listed in Ref. 19.

Nonuniform Field Problem; Quasistatics

The initial-boundary value problems with nonuniform field variables are examined with the developed computer code. As shown in Fig. 2, the square laminate has length a, and the hole is located in the center with the radius R. The stacking sequence of the composite laminate is $[0/\pm 45/90]_s$, and the traction loads are along the x axis. Considering the geometric and material symmetry, a quarter of the laminate is discretized by 1680 triangular finite elements.

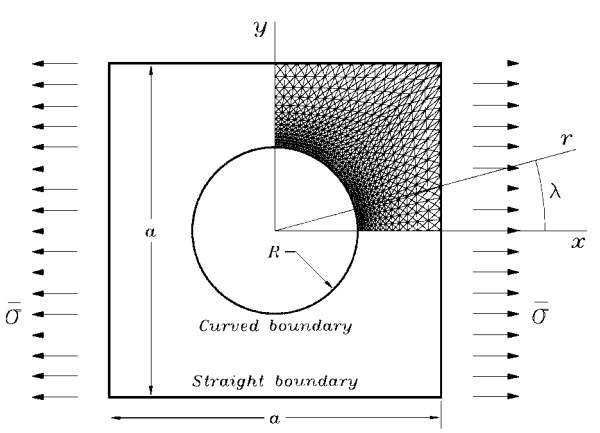

Fig. 2 Configuration of the composite laminate with a hole.

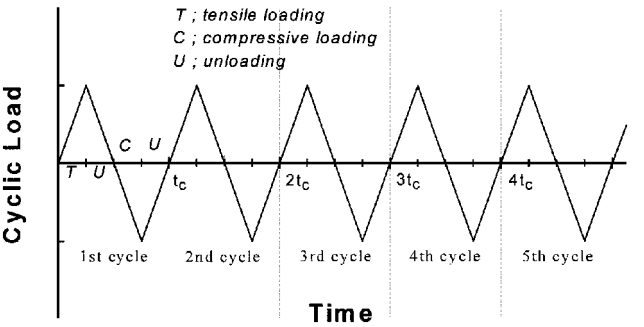

Fig. 3 Time history of cyclic loading applied to a composite laminate.

The applied traction force at each side is tension, unloading, compression, and unloading (T, U, C, U) during t_c for one cycle, as shown in Fig. 3. The upper bound of the cyclic load is 225 MPa and the lower bound −225 MPa. The traction force is successively loaded up to the 20th cycle. A total of five examples (STAT1–STAT5) are tested to compare the fully coupled quasistatic solutions with each other. The size of the laminate is $a = 4.0$ m and $R = 1.0$ m in STAT1–STAT3, $a = 0.4$ m and $R = 0.1$ m in STAT4, and $a = 0.04$ m and $R = 0.01$ m in STAT5. In addition, the load period t_c is different in each case. STAT1, STAT4, and STAT5 have a 4-s period. The period is 40 s in STAT2 and 400 s in STAT3.

Contour maps are drawn to view the distribution of viscoplastic work accumulated in the laminae. Figure 4 is the result of the developed work during 0–1 s; therefore, the tension load is applied in the first cycle of STAT1. The maximum value is predicted at the upper boundary of the hole in the 90-deg ply. Note that the dissipated viscoplastic work is one measure of the heating effect due to thermomechanical coupling. It is expected that the coupling effect may become apparent around the upper boundary of the hole.

To examine the thermomechanical coupling effect, the temperature changes from the base temperature θ_0 are predicted at a boundary point during the first four cycles. In Fig. 5, the cycle number is a dimensionless parameter of the current time t with reference to t_c. Because the laminates deform viscoplastically around the point, the upper bounds of temperature values increase gradually, except in STAT5.

Figure 6 shows the distribution of the temperature change θ_+ along the hole boundary. It can be seen that the patterns of the temperature distribution are different for each problem. They depend mainly on the heat conduction term in the energy conservation equation. If the load is applied at a higher rate, the viscoplastic work will be accumulated on a local area with less heat conduction. Therefore, the local heating effect lasts as in STAT1 or STAT2. The maximum temperature change is about 30°C after 20 cycles. When the number of repeated cycles is increased, the heating effect will be considerable. In contrast to these cases, the heating effect is relatively weak in STAT3 because of slower loading. By comparing STAT1, STAT4, and STAT5, one can see that the laminate size also plays an important role (keeping in mind that the conduction term is expressed with the second spatial derivatives). The coupling effect is negligible for a small laminate as in STAT5 because the thermal energy easily spreads to the surrounding.

Nonuniform Field Problem: Dynamics

When t_c has the same order as the fundamental period t_n for the initial elastic state of the composite laminate, dynamic analyses must be performed including the inertia term. As shown in Fig. 7, consider a laminate supported by rigid walls with the dimensions $a = 1.0$ m, $b = 0.09$ m, and $h = 0.01$ m. The stacking sequence is $[0/\pm 45/90]_s$. Only the right half is discretized with 480 triangular elements. The point force is cyclically applied with the range of $\pm P_{\max}$, as shown in Fig. 7.

The fundamental period t_n can be determined by solving the generalized eigenvalue problem of the free vibration for the elastic

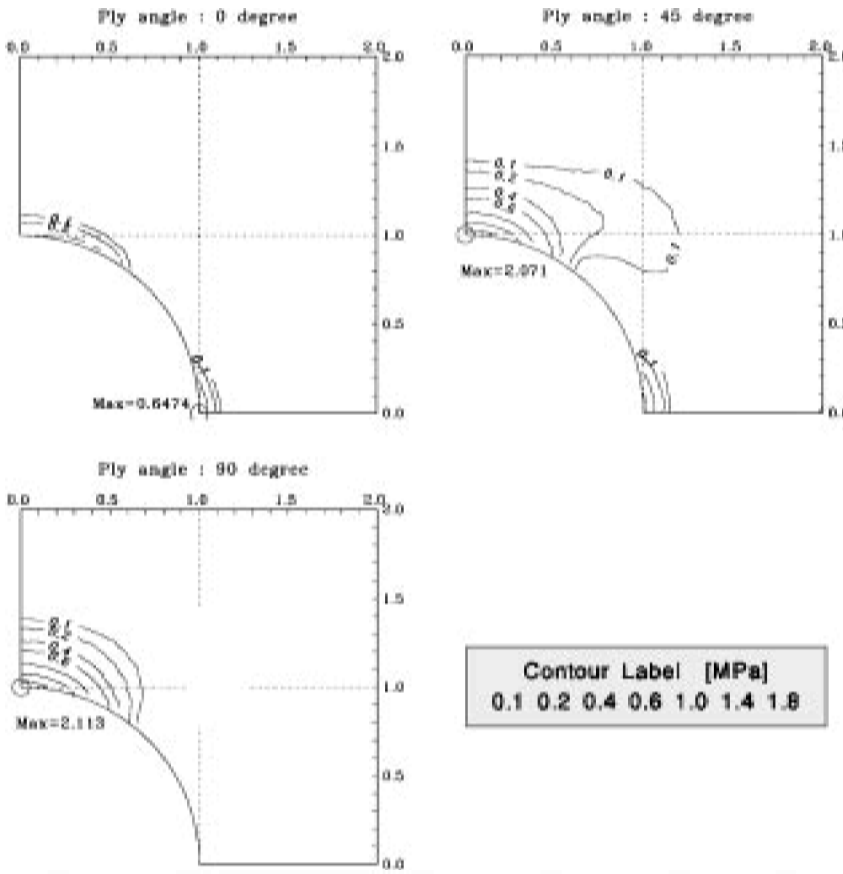

Fig. 4 Developed viscoplastic work during 0–1 s (1st cycle); STAT1.

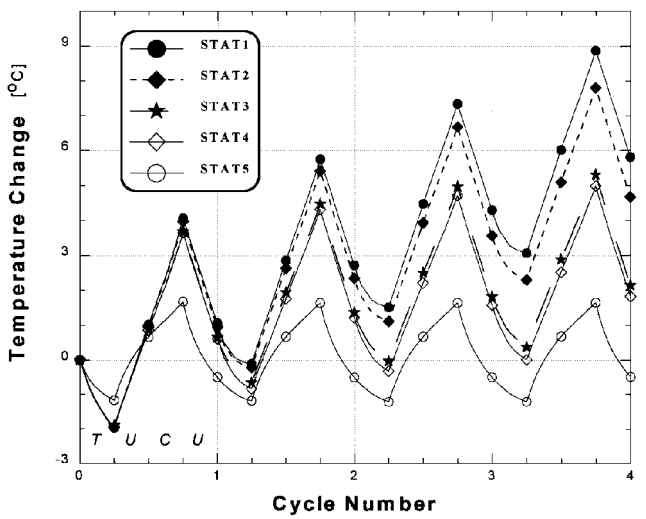

Fig. 5 Temperature change vs cycle number (t/t_c) up to the fourth cycle at (r, λ) = (R, 90 deg); STAT1–STAT5.

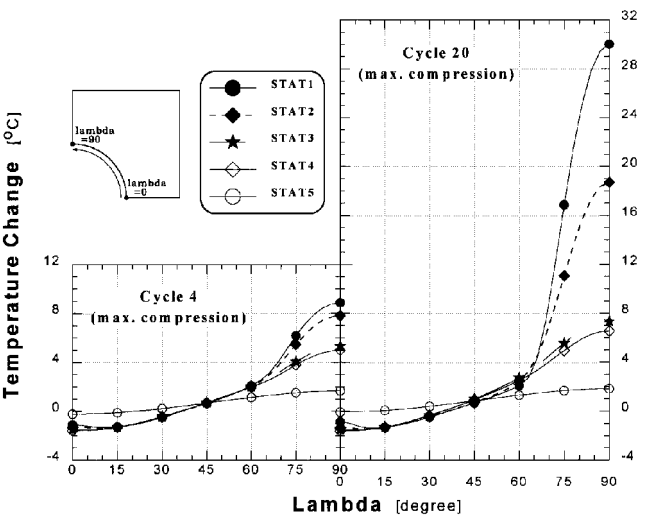

Fig. 6 Distribution of temperature change at t/t_c = 3.75 and 19.75 (max. compression); STAT1–STAT5.

deformation. For that purpose, Eq. (24) is reduced to the following form:

$$[K_U]\{\phi\} = \omega^2[M_U]\{\phi\} \tag{49}$$

Because only the lower modes need to be checked, the natural mode shapes for the four modes are shown in Fig. 8 with their periods $2\pi/\omega$. Note that the fundamental period t_n is equal to 1.566 ms.

Two examples (DYNA1 and DYNA2) are solved to show the coupled dynamic behavior of the viscoplastic composite. Because the fundamental mode is important in this case, t_c is changed with reference to t_n. In DYNA1, the load cycle t_c is 7.831 ms, five times

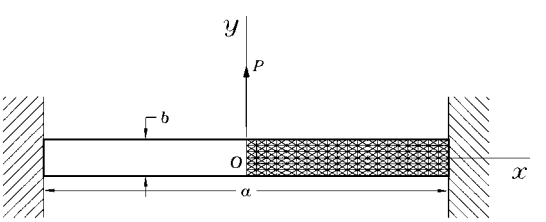

Fig. 7 Configuration of the composite laminate supported by rigid walls.

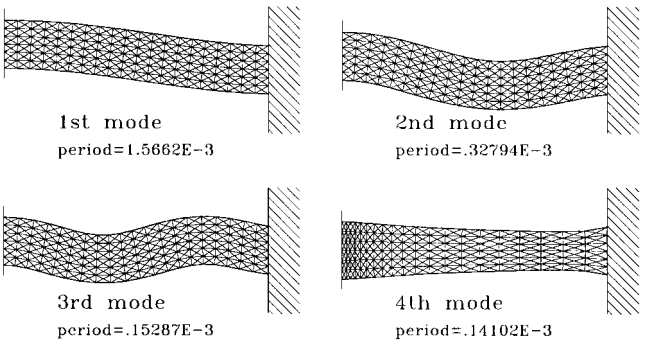

Fig. 8 Natural mode shapes and periods of the composite laminate.

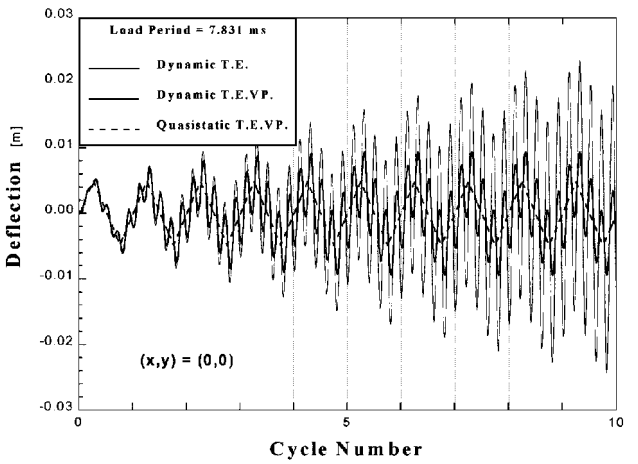

Fig. 9 Deflection vs cycle number (t/t_c) up to the 10th cycle at $(x, y) = (0, 0)$; DYNA1.

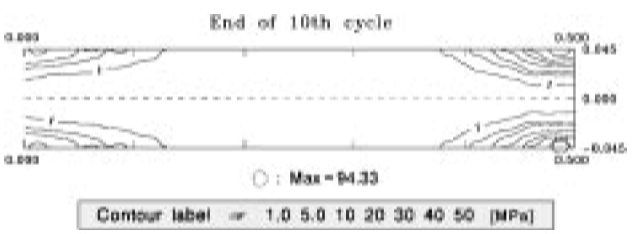

Fig. 10 Developed viscoplastic work at $t = 100t_c$; DYNA1.

that of the t_n, with $P_{\max} = 195.8$ kN. In DYNA2, the t_c is equal to t_n with $P_{\max} = 35.24$ kN. In numerical experiments, the relative errors for the convergence are fixed to 0.02%, and the subdivision number for the subincrementing technique is 100.

DYNA1 results are presented in Figs. 9–12. In Fig. 9, the deflection at the center of laminate is plotted with the cycle number. In the figures, T.E. is thermo–elasticity, and T.E.VP. is thermo–elasto–viscoplasticity. The curve of quasistatic (Q) T.E.VP. is also drawn to observe the characteristics of dynamic (D) T.E.VP. The deflection curve of Q.T.E.VP. linearly increases or decreases with constant amplitude, which implies that no viscoplastic deformation occurs. The result of D.T.E. means that the deflection steadily grows mainly due to the component of the first natural mode (the component of the first mode oscillates about five times per cycle). But the curve of D.T.E.VP. is in contrast to these curves. Though the difference between them is not obvious at the initial stage, the difference becomes outstanding after the third cycle as the viscoplastic deformation develops. Note that the viscoplastic deformation provides the source of damping in the thermomechanical system, so the range of deflection is confined within about 0.01 m.

To visualize the viscoplastic deformation in the laminate (as shown in Fig. 10), the contour maps of viscoplastic work per unit volume are drawn at $t = t_c$ and $10t_c$. A considerable amount of the irreversible work is developed in the upper and the lower area of the center and the right boundaries, mainly because the normal stress

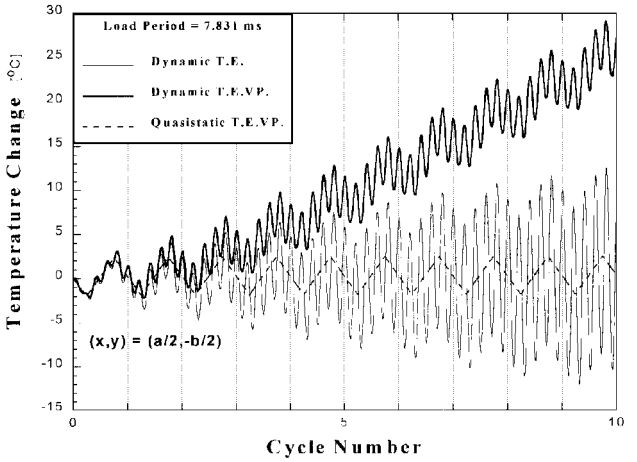

Fig. 11 Temperature change vs cycle number (t/t_c) up to the 10th cycle at $(x, y) = (a/2, -b/2)$; DYNA1.

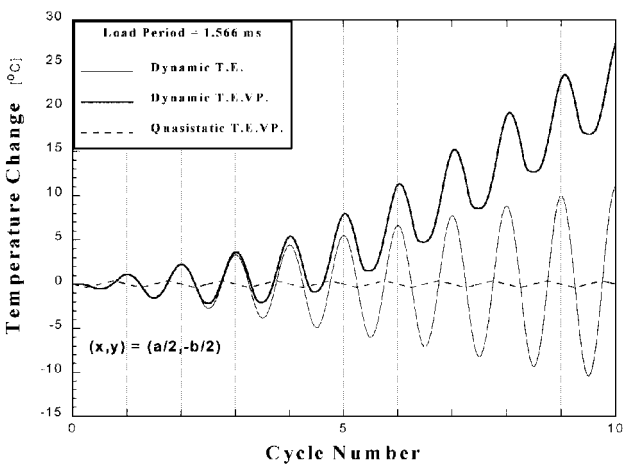

Fig. 12 Temperature change vs cycle number (t/t_c) up to the 10th cycle at $(x, y) = (a/2, -b/2)$; DYNA2.

σ_x is large in those regions. The other parts of the laminate deform elastically. The viscoplastic deformation dissipates mechanical energy into thermal energy, so that the dynamic motion of the laminate does not diverge.

The response of temperature change due to the coupling effect is shown in Fig. 11. The result of D.T.E. shows that the phases of heating and cooling are repeated proportionally to the deflection without any viscoplastic effect. The heating effect is serious in the D.T.E.VP. case. The maximum temperature change is about 30°C in the 10th cycle. This confirms that, to constrain a divergent motion, viscoplastic work is transformed to thermal energy, which is accumulated in the insulated system.

Finally, the temperature response of DYNA2 is plotted in Fig. 12. As expected, the coupling effect is noticeable for the D.T.E.VP. curve. The maximum temperature rise is about 25°C after the 10 cycles.

Conclusions

We set up the finite element formulation that enables thermo–elasto–viscoplastic analyses for composite materials focusing on the fully coupled thermomechanical situation. Through a series of numerical tests, it is concluded that the heating effect due to the irreversible viscoplastic work may be significant depending on the repeated cycles, the applied load levels, and the material properties. In quasistatic nonuniform field problems, especially, the thermal conduction in the energy equation can relieve the cyclic heating effect. On the other hand, in a dynamic environment, the viscoplastic work dissipates mechanical energy into thermal energy, which acts as a damping mechanism. These numerical studies give some guidelines for an analyst whether or not the fully coupled formulation should be adopted to adequately simulate the behavior of composite materials in a given thermomechanical environment.

Appendix: Matrix Notations

Various tensors are expressed by matrices in the 1–2 coordinates[12,19]:

$$\{\sigma\} = \lfloor \sigma_1 \quad \sigma_2 \quad \tau_{12} \rfloor^T, \qquad \{\varepsilon\} = \lfloor \varepsilon_1 \quad \varepsilon_2 \quad \gamma_{12} \rfloor^T \tag{A1}$$

$$[A] = \begin{bmatrix} \dfrac{1}{E_1} & \dfrac{-\nu_{12}}{E_1} & 0 \\ \dfrac{-\nu_{12}}{E_1} & \dfrac{1}{E_2} & 0 \\ 0 & 0 & \dfrac{1}{G_{12}} \end{bmatrix} \tag{A2}$$

$$\{\alpha\} = \lfloor \alpha_1 \quad \alpha_2 \quad 0 \rfloor^T \tag{A3}$$

$$\left[B_{[m_i]}\right] = V_{[m_i]} \begin{bmatrix} \dfrac{E_{[m]}}{E_1} & 0 & 0 \\ q_{[m_i]2}\nu_{[m]} - \nu_{12}\dfrac{E_{[m]}}{E_1} & q_{[m_i]2} & 0 \\ 0 & 0 & q_{[m_i]12} \end{bmatrix} \tag{A4}$$

$$\left[C_{[f]}\right] = \begin{bmatrix} \dfrac{E_{[f]1}}{E_1} & \dfrac{V_{[m]}}{E_1}\left(p_{[f]2}\nu_{[f]12}E_{[m]} - p_{[m]2}\nu_{[m]}E_{[f]1}\right) & 0 \\ 0 & p_{[f]2} & 0 \\ 0 & 0 & p_{[f]12} \end{bmatrix} \tag{A5}$$

$$\left\{\beta_{[f]}\right\} = -V_{[m]}\frac{E_{[f]1}E_{[m]}}{E_1}\lfloor \alpha_{[f]1} - \alpha_{[m]} \quad 0 \quad 0 \rfloor^T \tag{A6}$$

$$\left[D_{[f_i]}\right] = V_{[m_i]}\frac{E_{[f]1}}{E_1}\begin{bmatrix} E_{[m]} & 0 & 0 \\ 0 & 0 & 0 \\ 0 & 0 & 0 \end{bmatrix} \tag{A7}$$

$$\left[C_{[m_i]}\right] = \begin{bmatrix} \dfrac{E_{[m]}}{E_1} & p_{[m_i]2}\nu_{[m]} - \nu_{12}\dfrac{E_{[m]}}{E_1} & 0 \\ 0 & p_{[m_i]2} & 0 \\ 0 & 0 & p_{[m_i]12} \end{bmatrix} \tag{A8}$$

$$\left\{\beta_{[m]}\right\} = V_{[f]}\frac{E_{[f]1}E_{[m]}}{E_1}\lfloor \alpha_{[f]1} - \alpha_{[m]} \quad 0 \quad 0 \rfloor^T \tag{A9}$$

$$\left[D_{[m_{ij}]}\right] = \left(V_{[m_j]}\frac{E_{[m]}}{E_1} - \delta_{ij}\right)\begin{bmatrix} E_{[m]} & 0 & 0 \\ 0 & 0 & 0 \\ 0 & 0 & 0 \end{bmatrix} \tag{A10}$$

where p is the stress variation factor and q the strain contribution factor.

References

[1]Tenney, D. R., Lisagor, W. B., and Dixon, S. C., "Materials and Structures for Hypersonic Vehicles," *Journal of Aircraft*, Vol. 26, No. 11, 1989, pp. 953–970.

[2]Thornton, E. A. (ed.), *Thermal Structures and Materials for High-Speed Flight*, Vol. 140, Progress in Astronautics and Aeronautics, AIAA, Washington, DC, 1992.

[3]Robinson, D. N., and Duffy, S. F., "Continuum Deformation Theory for High-Temperature Metallic Composites," *Journal of Engineering Mechanics*, Vol. 116, No. 4, 1990, pp. 832–844.

[4]Lee, K. D., and Krempl, E., "An Orthotropic Theory of Viscoplasticity Based on Overstress for Thermomechanical Deformations," *International Journal of Solids and Structures*, Vol. 27, No. 11, 1991, pp. 1445–1459.

[5]Gates, T. S., and Sun, C. T., "Elastic/Viscoplastic Constitutive Model for Fiber Reinforced Thermoplastic Composites," *AIAA Journal*, Vol. 29, No. 3, 1991, pp. 457–463.

[6]Ha, S. K., Wang, Q., and Chang, F. K., "Modeling the Viscoplastic Behavior of Fiber-Reinforced Thermoplastic Matrix Composites at Elevated Temperatures," *Journal of Composite Materials*, Vol. 25, 1991, pp. 334–374.

[7]Saleeb, A. F., and Wilt, T. E., "Analysis of the Anisotropic Viscoplastic-Damage Response of Composite Laminates—Continuum Basis and Computational Algorithms," *International Journal for Numerical Methods in Engineering*, Vol. 36, No. 10, 1993, pp. 1629–1660.

[8]Dvorak, G. J., and Bahei-El-Din, Y. A., "Plasticity Analysis of Fibrous Composites," *Journal of Applied Mechanics*, Vol. 49, June 1982, pp. 327–335.

[9]Aboudi, J., "Micromechanical Analysis of Composites by the Method of Cells," *Applied Mechanics Reviews*, Vol. 42, No. 7, 1989, pp. 193–221.

[10]Hall, R. B., "Matrix-Dominated Thermoviscoplasticity in Fibrous Metal–Matrix Composite Materials," Ph.D. Dissertation, Rensselaer Polytechnic Inst., Troy, NY, 1990.

[11]Kim, S. J., and Cho, J. Y., "Role of Matrix in Viscoplastic Behavior of Thermoplastic Composites at Elevated Temperature," *AIAA Journal*, Vol. 30, No. 10, 1992, pp. 2571–2573.

[12]Kim, S. J., and Shin, E. S., "A Thermoviscoplastic Theory for Composite Materials by Using a Matrix-Partitioned Unmixing–Mixing Scheme," *Journal of Composite Materials*, Vol. 30, No. 15, 1996, pp. 1647–1669.

[13]Oden, J. T., Bhandari, D. R., Yagawa, G., and Chung, T. J., "A New Approach to the Finite-Element Formulation and Solution of a Class of Problems in Coupled Thermoplasticity of Crystalline Solids," *Nuclear Engineering Design*, Vol. 24, 1973, pp. 420–430.

[14]Argyris, J. H., Vaz, L. E., and William, K. J., "Integrated Finite Element Analysis of Coupled Thermoviscoplastic Problems," *Journal of Thermal Stresses*, Vol. 4, 1981, pp. 121–153.

[15]Ghoneim, H., and Matsuoka, S., "Thermoviscoplasticity by Finite Element: Tensile and Compression Test," *International Journal of Solids and Structures*, Vol. 23, No. 8, 1987, pp. 1133–1143.

[16]Banas, A., Hsu, T. R., and Sun, N. S., "Coupled Thermoelastic–Plastic Stress Analysis of Solids by Finite-Element Method," *Journal of Thermal Stresses*, Vol. 10, 1987, pp. 319–344.

[17]Allen, D. H., "Thermomechanical Coupling in Inelastic Solids," *Applied Mechanics Reviews*, Vol. 44, No. 8, 1991, pp. 361–373.

[18]Odabas, O. R., and Sarigul-Klijn, N., "Thermomechanical Coupling Effects at High Flight Speeds," *AIAA Journal*, Vol. 32, No. 2, 1994, pp. 425–430.

[19]Shin, E. S., Yoon, K. J., and Kim, S. J., "Elasto-Viscoplastic Analysis of Composite Materials Considering Thermomechanical Coupling Effects," *Proceeding of the AIAA 37th Structures, Structural Dynamics, and Materials Conference* (Salt Lake City, UT), AIAA, Washington, DC, 1996, pp. 2285–2293 (AIAA Paper 96-1578).

[20]Germain, P., Nguyen, Q. S., and Suquet, P., "Continuum Thermodynamics," *Journal of Applied Mechanics*, Vol. 50, 1983, pp. 1010–1020.

[21]Chan, K. S., Lindholm, U. S., and Bodner, S. R., "Constitutive Modeling for Isotropic Materials (HOST)—Final Report," NASA CR 182132, 1988.

[22]Bathe, K. J., *Finite Element Procedures*, Prentice–Hall International, 1996.

[23]Zienkiewicz, O. C., and Taylor, R. L., *The Finite Element Method*, 4th ed., Vol. 2, McGraw–Hill, New York, 1991, pp. 352–361.

[24]Bass, J. M., and Oden, J. T., "Numerical Solution of the Evolution Equations of Damage and Rate-Dependent Plasticity," *International Journal of Engineering Science*, Vol. 26, No. 7, 1988, pp. 713–740.

A. M. Waas
Associate Editor